1.06μm picosecond pulsed, normal dispersion pumping for generating efficient broadband infrared supercontinuum in meter-length single-mode tellurite holey fiber with high Raman gain coefficient

Jindan Shi, Xian Feng, Peter Horak, Kangkang Chen, Peh Siong Teh, Shaif-ul Alam, Wei H. Loh, David J. Richardson, Morten Ibsen

***Abstract*—We investigate efficient broadband infrared supercontinuum generation in meter-length single-mode small-core tellurite holey fiber. The fiber is pumped by 1.06μm picosecond pulses in the normal dispersion region. The high Raman gain coefficient and the broad Raman gain bands of the tellurite glass are exploited to generate a cascade of Raman Stokes orders, which initiate in the highly normal dispersion region and quickly extend to longer wavelengths across the zero dispersion wavelength with increasing pump power. A broadband supercontinuum from 1.06μm to beyond 1.70μm is generated. The effects of the pump power and of the fiber length on the spectrum and on the power conversion efficiency from the pump to the supercontinuum are discussed. Power scaling indicates that using this viable normal dispersion pumping scheme, 9.5W average output power of infrared supercontinuum and more than 60% conversion efficiency can be obtained from a 1m-long tellurite fiber with a large-mode-area of 500μm^2.**

***Index Terms*—Nonlinear optics, Non-silica glass fiber, Supercontinuum generation, Raman scattering**

I. Introduction

Supercontinuum (SC) is generated when a combination of nonlinear processes act together upon a pump beam in order to cause severe spectral broadening of the original pump [1]. Compact all-fiber based single-mode broadband infrared supercontinuum sources providing output across the range from 1μm to 5μm are desired for various applications in a diverse range of fields, including airborne light detection and ranging (LIDAR), optical coherence tomography (OCT), frequency metrology, fluorescence lifetime imaging, and gas sensing.

Efficient supercontinuum generation (SCG) in optical fibers relies critically upon several parameters of the nonlinear fiber employed, including (i) the effective nonlinearity γ ($=2\pi n_2/(\lambda A_{eff})$, where n_2 is the nonlinear refractive index of the core glass, λ is the wavelength and A_{eff} is the effective mode area of the fiber), (ii) the group velocity dispersion (GVD) at the pump wavelength and the dispersion profile, and (iii) the effective length of the fiber, L_{eff} ($=[1-\exp(-\alpha_p \cdot L)]/\alpha_p$, where α_p represents the optical loss of the fiber at the pump wavelength, and L is the fiber length).

In order to obtain the broadest supercontinuum, the most efficient scheme is to pump the fiber within the anomalous dispersion regime [2]. This means that it is necessary either: to find a suitable pump source operating at a wavelength longer than the zero dispersion wavelength (ZDW) of the fiber; or to suitably engineer the dispersion profile of the fiber so that the ZDW matches the preferred commercial laser pump sources. The latter can frequently be realized using holey fiber (HF) technology [3]. For example, it has been shown that it possible to engineer the ZDW(s) of silica glass based HF over a very broad wavelength range (anywhere down to the green regions of the spectrum) via suitable control of the air-fill fraction and the lattice structure of the air holes in the microstructured cladding. This is possible due to the wavelength-scale features of the microstructured cladding and the large index-contrast between the air and the background material. As a result, it becomes possible to fabricate a silica fiber with a ZDW slightly shorter than the wavelength of most common pump laser sources – for example down to 1μm to match the operating wavelength of the ytterbium doped fiber laser which is merging as a pump laser of choice for many applications. However note that in order to achieve a ZDW much shorter than the material dispersion wavelength generally requires a fiber with a very small core since a large positive waveguide dispersion is required in this case to compensate the large negative dispersion of the core material. Such ZDW-shifted fibers are therefore generally quite nonlinear and the further the pump wavelength from the material ZDW the smaller the core and the more highly nonlinear and more prone to optical damage the fiber becomes.

Achieving maximum bandwidth is often not the only concern when designing a practical SC source. The maximum output power and spectral intensity are frequently equally important issues. In this regard the use of anomalous dispersion pumping at wavelengths much shorter than the material dispersion wavelength of the fiber can be restrictive due to the small fiber core size required to achieve ZDW-shifted operation. The dispersion of weakly guiding large core fibers is dominated by the core material dispersion which typically occurs at long wavelength relative to the most convenient high power pump sources. Investigating techniques that allow pumping deep in the normal dispersion regime are thus of great interest.

The authors are with Optoelectronics Research Centre, University of Southampton, Southampton, SO17 1BJ, UK. (phone: +44 (0)23 80593836; fax: +44 (0)23 80593149; e-mail: xif@orc.soton.ac.uk).

The pump requirements and general mechanism of broadband SC generated through normal dispersion pumping are as follows: first, the pump pulse duration should be relatively long, e.g. a few picoseconds (ps) or longer; in this case stimulated-Raman scattering (SRS) tends to dominate and typically a series of cascaded discrete Stokes lines will appear until the ZDW of the fiber is reached; finally, with sufficiently high pump power, the SC spectrum will cross the ZDW and then rapidly expand to much longer wavelengths due to nonlinear effects such as modulation instability (MI), four wave mixing (FWM), and soliton fission [2] which now dominate in this dispersion regime. Note that with the normal dispersion pumping, if the pulse duration is several hundreds of femtoseconds (fs) or less, self-phase-modulation (SPM) will dominate the pulse broadening mechanism and the spectral bandwidth will be narrow due to the approximately symmetric temporal pulse broadening [4]. To realize an efficient and broadband SC using the 1.06μm normal dispersion pumping scheme, the length of the nonlinear fiber should be short in order to minimize the walk-off effect, which is significant at high normal dispersion. To circumvent this, the core material should possess a high Raman gain coefficient, a large Raman gain bandwidth, and a high nonlinear refractive index n_2.

Tellurite (TeO_2 based) glass is an ideal candidate with a Raman gain coefficient about 30 times higher than that of silica and a Raman gain bandwidth which is almost twice that of silica [5]. Moreover, the n_2 of tellurite glass is typically one order of magnitude higher than that of pure silica [6]. The ZDW of the tellurite bulk glass is typically around 2.0-2.3μm [7], thus a tellurite fiber with relatively large core diameter will typically exhibit normal dispersion at 1.06μm, unless the fiber is an air-suspended-core (ASC) HF with a submicron-size core and correspondingly large waveguide dispersion [8]. In addition, a few works on generating broadband SC in tellurite HFs have been reported (e.g., Ref. [8]) using near-zero or anomalous dispersion pumping scheme, because the main focus on those works is to maximize the bandwidth of the generated SC spectrum rather than taking the feasibility of generating SC with the practically usable power level into consideration as the first priority.

In this work, we first investigated the Raman gain coefficient of the widely studied sodium zinc tellurite glass and of fused silica glass for reference, based on the measured spectrum of spontaneous Raman scattering. Next, an air-suspended-core (ASC) tellurite holey fiber (HF) with a ZDW of 1.38μm was fabricated with the same glass composition. A 20 ps pulsed laser source at 1.06μm, at which the HF has high negative dispersion value of -320ps/nm/km, was employed to study SCG from this tellurite ASC HF. Cascaded Raman Stokes was observed under low average pump power, and the spectrum quickly evolved to form a supercontinuum across the ZDW of the fiber by increasing pump power. Comparing the output spectra for different pump powers and different fiber lengths shows that the efficient generation of broadband SC with normal dispersion pumping is mainly attributed to the high Raman gain coefficient and the large Raman gain bandwidth of the tellurite glass. Based on the facet damage threshold of the fiber in the experiment, we calculate that it should be feasible to scale the average power of the SC to near 10W, corresponding to a mean spectral density of 15mW/nm, in a 1m-long large-mode-area (LMA) ($500\mu m^2$) tellurite fiber.

II. Raman Gain Coefficient of Tellurite Glass

A. Preparation of bulk Tellurite glass

The tellurite glass studied here was made in house based on the composition of $75TeO_2$-$20ZnO$-$5Na_2O$ (mol.%) (TZN) [9, 10]. The glass has a refractive index of 2.0 at 1.06μm and a glass transition temperature T_g of 300°C. High purity commercial chemicals of tellurium dioxide (TeO_2, purity: 99.9995%, Alfa Aesar), zinc oxide (ZnO, purity: 99.9995%, Alfa Aesar), and sodium carbonate (Na_2CO_3, purity: 99.997%, Alfa Aesar) were used as raw materials for glass melting. A batch of ~30grams was well-mixed first and then melted in a gold crucible at 800ºC for 45 minutes. Pure oxygen gas was purged into the furnace during the melting. The melt was then cast into a stainless steel mold which was preheated around the glass transition temperature (T_g). The glass and the mold were held around T_g for 2 hours to remove the thermal stress inside, and then cooled down to room temperature. The glass sample was grounded down to the dimensions of 20 x 10 x 3 mm and the two largest parallel faces were polished to optical quality.

B. Calculation of the Raman gain coefficient of bulk glasses

The depolarized spontaneous Raman scattering spectra of the TZN glass and a reference pure silica glass were measured by a micro-Raman spectrometer (RENISHAW Ramanscope) using a He-Ne laser (633nm) as pump source. With the assistance of a CCD camera, it was ensured that the laser beam was focused on the top surface of the sample. The Raman spectra were recorded from $200cm^{-1}$ to $1000cm^{-1}$ with a resolution of $1cm^{-1}$.

The reduced Raman intensity spectra were obtained by dividing the spontaneous Raman spectra by the thermal population factor of $(1+n_b)$, where n_b is the Bose-Einstein thermal factor [11,12] ($n_b = [\exp(h\upsilon/kT)-1]^{-1}$, where h is Planck's constant, υ is the Raman shift frequency, T is the temperature for the measurement, and k is Boltzmann's constant). The reduced Raman intensity spectrum exhibits a line-shape which is close to that of stimulated Raman scattering [12].

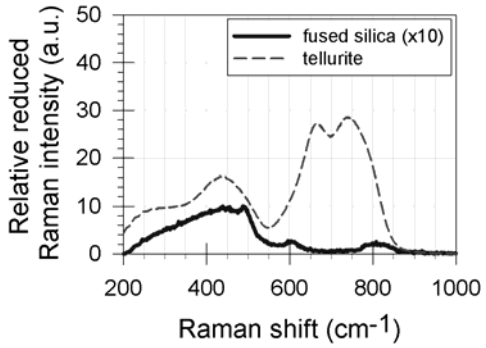

Fig. 1: Relative reduced Raman intensities of TZN glass and referenced pure silica glass, normalized to the peak intensity of silica at $440cm^{-1}$.

In order to evaluate the Raman gain coefficient of the tellurite glass, the reduced Raman intensity is normalized by the peak Raman intensity of pure silica glass at 440cm^{-1}. Fig.1 shows the relative reduced Raman intensity spectra of the samples. The Raman vibration at 433cm^{-1} is associated with the glass Te-O-Te chain unit's symmetric stretching mode, and the spectral features at 665cm^{-1} and 741cm^{-1} are due to the vibration of the TeO_4 bipyramidal structural arrangement and the TeO_{3+1} (or distorted TeO_4) unit, respectively [5].

Since the Raman gain coefficient g is related to the differential cross section as: $g = \sigma\lambda_s^3/(c^2hn^2)$ [13] (σ is the differential cross section, λ_s is the Stokes wavelength, and n is the refractive index of the glass), we obtained the Raman gain coefficient of the tellurite glass by:

$$g_{TZN} = g_{p\_SiO_2} \cdot \sigma_{TZN\_relative} \cdot (\frac{n_{SiO_2}}{n_{TZN}})^2 \cdot (\frac{\lambda_{s\_TZN}}{\lambda_{s\_SiO_2}})^3, \qquad (1)$$

where $g_{p\_SiO_2}$ is the peak Raman gain coefficient of the silica glass and $\sigma_{TZN\_relative}$ is the ratio of the differential cross section of the tellurite glass to that of silica. The relative differential cross section can be obtained by multiplying the relative reduced Raman intensity with a correction factor F, which takes the changes in the scattering geometry and the intensity related to the refractive index of the samples into account [14]. We calculated the F factor using the method presented in Ref. [12]. Table 1 shows the Raman gain coefficient of TZN glass for pump wavelengths of 633nm and 1060nm, respectively. The Raman gain coefficient was calculated through Equation (1) by using the relative differential cross section, the gain coefficient of silica and the refractive index also shown in Table 1. The reference peak gain of silica with pump wavelengths of 633nm and 1064nm, was converted from the gain coefficient of 1.86 x 10^{-11} cm/W with 532nm pumping [13] using its dependence on the pump wavelength as $1/\lambda_p$ [13]. It is seen that with the pump of 1060nm the Raman gain coefficient of TZN glass at the 741cm^{-1} Raman shift is 35 times higher than that of pure silica glass at 440cm^{-1}.

Table 1. Refractive index at 633nm, correction factor F, peak wave number, peak relative reduced Raman intensity, peak relative differential cross section and peak Raman gain coefficient of investigated glasses with pumps at 633nm and 1064nm.

Glass	SiO_2	TZN		
Refractive index (n@633nm)	1.457	2.0335		
Correction factor (F)	1	2.154		
Peak wave number (cm^{-1})	440	433	665	741
Relative reduced Raman intensity	1	16	26.9	28.2
Relative differential cross section	1	34.46	57.94	60.74
Raman gain coefficient @633nm (x10^{-11} cm/W)	1.56	27.69	50.29	54.07
Raman gain coefficient @1064nm (x10^{-11} cm/W)	0.93	16.47	29.92	32.17

In principle, since Raman scattering is a polarization-dependent effect, the polarized spontaneous Raman spectrum rather than the depolarized spontaneous Raman spectrum should be utilized for the calculation of the Raman gain coefficient of the bulk glass. However, for both tellurite glass and silica glass, the intensity of the Raman scattering is dominated by the parallel polarization (VV) and the intensity of the perpendicular polarization (VH) is typically only 5% of the former intensity [13]. As a result, the depolarized spontaneous Raman spectrum gives a relative reduced Raman intensity almost identical to the one obtained from the polarized spontaneous Raman spectrum.

III. FIBER FABRICATION AND FUNDAMENTAL PROPERTIES

In order to understand the mechanism of SC generation with the involvement of SRS in tellurite fiber under 1.06μm normal dispersion pumping, a single-mode tellurite HF with an air-suspended-core (ASC) was used for the experiment. The tellurite ASC HF with a composition of 75TeO_2-20ZnO-5Na_2O (mol.%) was made in-house using the extrusion method [10]. Fig.2(a) shows Scanning Electron Microscope (SEM) microphotographs of the cross-section of the fiber. It is seen that the fiber has an outer diameter (OD) of 250μm. A triangular core with an effective mode area (A_{eff}) of 2.6μm^2 is isolated from the outer glass jacket by three 7.4±0.2μm long and 180±20nm thin supporting struts.

Single-mode laser radiation at various wavelengths was respectively launched into one facet and the near-field spatial mode guidance characteristics of the fiber investigated by imaging the output mode onto a CCD camera. The fiber length used here is 1.35m. Fig.2(b) shows the near-field images from the HF from visible region (476nm and 514.5nm laser lines from an Argon laser; 635nm line from a single-mode fiber-pigtailed laser diode) to 1.06μm (see the source description in Section IV). It is observed that, at 476nm the fiber core is capable of supporting a few higher-order modes. The core appears to support fewer modes at 514.5nm and 635nm. Robust singlemode guidance is observed at 1.06μm. The numerical simulation shows that at 1.06μm the normalized frequency V number of the HF is ~10, indicating that multiple modes should be guided in the HF. In our experiment, higher-order modes were not excited or were not easily to be excited in such a small-core fiber with a short length. At 1.06μm the observed single mode guidance is robust and not sensitive to the launching condition. Thus this HF is effectively single-moded at 1.06μm.

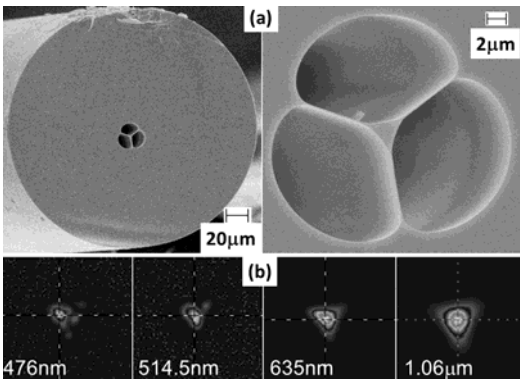

Fig.2: (a) SEM photographs of the fabricated tellurite ASC HF with 2.6μm core diameter; (b) Observed near-field images from the output end of the ASC HF at 476nm, 514.5nm, 635nm and 1.06μm respectively.

The propagation loss of the HF was measured to be 2.3±0.2dB/m at 1.06μm and 1.9±0.2dB/m at 1.55μm by the cutback method, respectively. The loss spectrum from 600nm to 1700nm was also measured using the cutback method too. A 1watt tungsten halogen lamp as the broadband source, and the spectrum traces from 600 to 1700 nm were recorded by an optical spectrum analyzer (Ando AQ-6315A). Note that in the measurement of the spectrum (600-1700nm) and the scatter loss values (at 1.06μm and 1.55μm), the total cutback length between 0.5-2m and at least four cutback measurements were done. Fig.3 shows the measured loss spectrum and the measured loss values at 1.06μm and 1.55μm. It is seen that the loss spectrum from 1.0-1.65μm is relatively flat and ranging between 2-3dB/m.

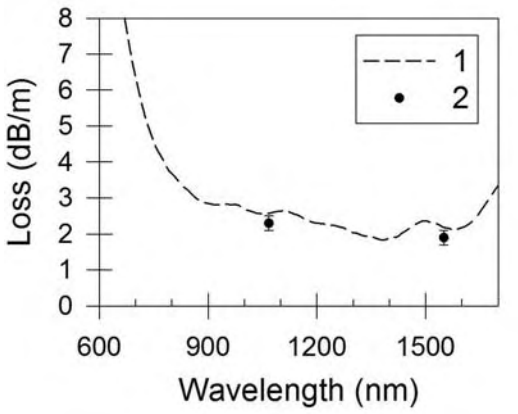

Fig.3: Measured loss spectrum and the loss values (scatter) at 1.06μm and 1.55μm of the tellurite ASC HF

Fig.4 shows the dispersion profiles of the tellurite ASC HF (calculated) and of the bulk tellurite glass. The ZDW of the HF is shifted to 1.38μm from the 2.15μm in the bulk, due to the large waveguide dispersion of the small air-suspended core [15]. At 1.06μm the dispersion of the HF is -320ps/nm/km. Note that although this fiber was made in 2004 and then stored in the laboratory without any special care, no degradation in terms of the mechanical strength and the optical properties has been observed on the fiber in this experiment, indicating the excellent chemical durability of the chosen tellurite glass composition.

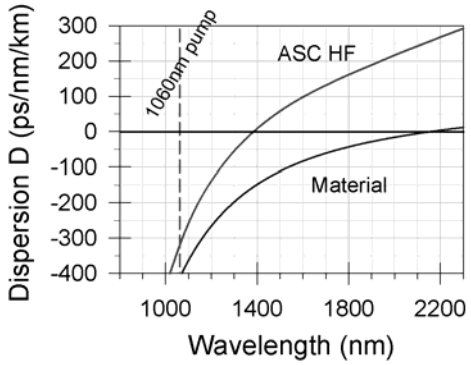

Fig.4: Dispersion curves of the fabricated tellurite ASC HF (calculated) and of the bulk material. The vertical line indicates the pump wavelength.

IV. SRS AND SC GENERATED IN TELLURITE FIBER

A. Experimental set-up

The experimental setup for SC generation in the tellurite ASC HF is shown in Fig. 5. A 1.06μm Yb-doped all-fiber MOPA with pulse duration of 20ps and repetition rate of 14.4MHz [16] was used as the pump source. The optical output of the MOPA was coupled into the small core of the tellurite HF using free-space lens coupling. A CCD camera was used to monitor the near-field image of the output end of the tellurite HF to ensure that the pump light was coupled into the core. Water-cooling was applied at the input end of the tellurite HF to remove the generated heat.

Under low pump power the launching efficiency, i.e., the ratio of the actual pump power launched into the fiber core to the pump power before the focusing lens in front of the fiber, was measured to be 39%. This launching efficiency includes the transmission loss of the focus lens, the Fresnel reflection loss at both ends of the high-index tellurite glass fiber, the loss induced by the mismatch of the focused pump spot with the mode area of the ASC HF. It is feasible to enhance the launching efficiency significantly by splicing the tellurite fiber with silica fiber so that the Fresnel reflection loss is reduced due to the smaller index contrast between silica (n=1.45) and tellurite (n=2.0) than that between air and tellurite glass. The generated output spectra from the fiber were recorded by an optical spectrum analyzer (OSA) (Agilent 86140B) with a resolution bandwidth of 0.5nm. A power meter was used to measure the average power of the SC at the output end of the HF for each value of the launched average pump power.

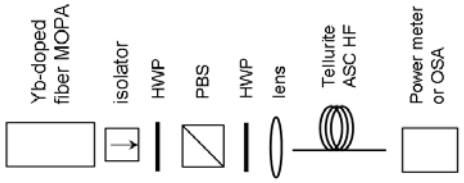

Fig.5: Schematic of experimental setup for SCG in tellurite ASC HF; HWP: half-wave plate; PBS: Polarizing Beamsplitter.

In the experiment, the fiber initially had a length of 1.35±0.02m, and the generated SC spectra were observed under launched average pump powers of 16.0, 24.6, 33.9, 58.5, 80.0, and 128.7mW. The fiber was then cut to a length of 0.50±0.02m and the generated SC spectra were measured using the same launched average pump powers.

B. Generation of first Raman Stokes and anti-Stokes order

According to the reduced Raman intensity of TZN glass shown in Fig.1, with pumping at 1060nm the first Raman Stokes order in the tellurite ASC HF should have three peaks at 1111nm, 1140nm, and 1150nm, while the first Raman anti-Stokes order from the tellurite glass fiber should have three peaks at 1013nm, 990nm, and 983nm.

At 1060nm, the effective length L_{eff} of the fiber with actual lengths of 1.35m and 0.50m is calculated to be 0.96m and 0.42m, respectively. The walk-off length ($L_W=T_0/|\beta_1(\lambda_p)-\beta_1(\lambda_S)|$, where T_0 is the duration of the pulse (20ps), and $\beta_1(\lambda_p)-\beta_1(\lambda_S)$ is the separation between the pump and the Stokes waves) is calculated to be 0.75m between 1060nm and

1150nm. Since the L_{eff} of the fiber with lengths of 1.35m and 0.50m are comparable to the L_W between the first order Stokes and pump waves, the walk-off effect will have some impact on the SRS generation, especially for the longer length.

Fig.6 illustrates the evolution of generating the first order Raman Stokes and anti-Stokes peaks from the fibers with lengths of 1.35m (top) and 0.5m (bottom) for increasing launched average pump power.

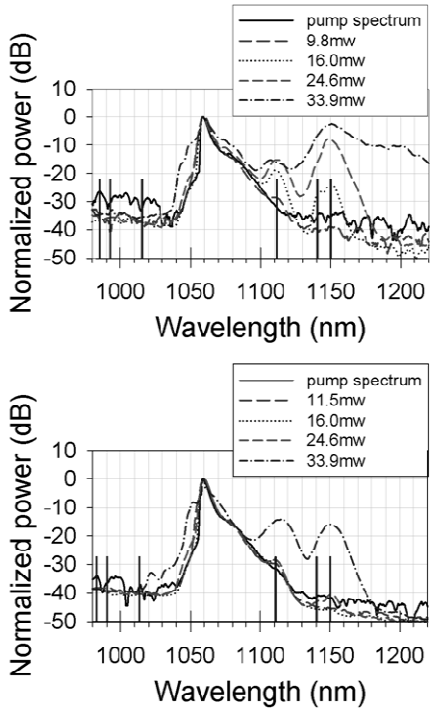

Fig.6: Observed first-order SRS in tellurite HF for different launched average pump powers (top: fiber length 1.35m; bottom: fiber length 0.50m). The vertical lines represent the individual positions of the first order Stokes and anti-Stokes peaks.

For the HF with 1.35m length, the first Stokes order appears when the launched average pump power is around 9.8mW, corresponding to a peak power of 34W. When the launched average pump power increases to 24.6mW, the first order Stokes wave, which has an identical profile to that of bulk glass, is significantly enhanced. In the case of 0.50m-long fiber, the launched average pump power needs to be as high as 33.9mW to reach similar enhancement for the first order Stokes wave as in the 1.35m fiber, for the shorter fiber has a smaller Raman gain.

For the 1.35m-long fiber, the second order Stokes is generated and the spectrum extends beyond 1200nm with a launched average pump power of 33.9mW. With the same pump power for the 0.50m long fiber, two peaks belonging to the first order Stokes can be seen in Fig.6 (bottom) but the spectrum does not extend across 1180nm. Additionally, at this power level, a broadening of the spectrum on both sides of the pump is observed, due to the strong SPM effect. With a further increase of the launched average pump power the relative intensity of the Stokes peak at 741cm^{-1} keeps growing but the peak at 433cm^{-1} appears to be saturated. This is because the Stokes components at the higher frequency acts as pump for the lower frequency Stokes components. This is in agreement with the observation for silica glass fibers [4]. On the other hand, the first anti-Stokes order appears at ~1020nm, rather than the calculated 1013nm, in the 0.5m long fiber, but it does not show up at all for the 1.35m long fiber. This is mainly because the Raman gain profile is anti-symmetric, which is very different from the FWM based symmetric parametric gain profile, so that the frequency components on the anti-Stokes side of the pump are in principle converted back to longer wavelengths by consecutive Raman processes.

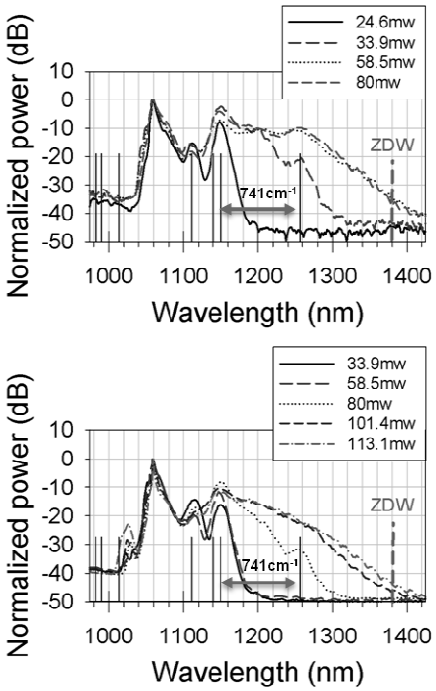

Fig.7: Observed Raman assisted SCG in the normal dispersion region of tellurite HF for different launched average pump powers (top: fiber length 1.35m; bottom: fiber length 0.50m). The vertical lines represent the individual positions of the first order Stokes/anti-Stokes and second order Raman Stokes peaks corresponding to the 741cm^{-1} Raman line. The dashed line at 1.38μm represents the ZDW of the tellurite HF.

C. Generation of higher-order Raman Stokes and anti-Stokes in the normal dispersion region

By further increasing the launched pump power, higher-order Stokes towards the longer wavelengths can be observed. Fig.7 illustrates the spectra of the generated higher order Raman Stokes, which extend towards the ZDW of the tellurite ASC HF. The wavelengths of the second and third orders of the Raman Stokes peak at 741cm^{-1} are calculated to be 1257nm and 1386nm, respectively. As seen in Fig.7, for both lengths of fiber, the spectrum appears much flatter than that of the first order Raman Stokes. This is very different from the discrete cascaded Raman lines observed in a 1km-long silica glass fiber [17]. We attribute such a continuum rather than discrete Raman Stokes lines here to (1) the much higher Raman gain coefficient and much broader Raman bands of tellurite glass compared to those of silica and (2) the nature of the multiple Raman peaks of tellurite glass.

Similar to Fig.6, it is seen in Fig.7 that the anti-Stokes at ~1.02μm only appears in the shorter fiber rather than in the longer fiber, arising from the nature of self-shifting of SRS to longer wavelengths. The 1.35m-long fiber, which has higher

Raman gain than the 0.50m-long fiber, can be viewed as utilizing the output power from the first 0.50m-long segment as the pump for the following 0.85m-long segment.

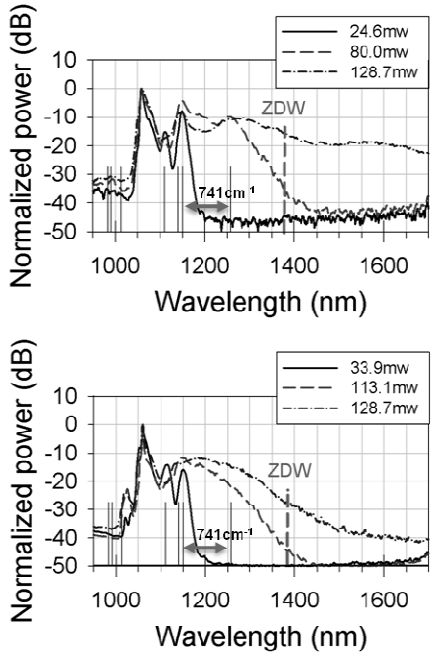

Fig.8: Observed Raman assisted SCG into the anomalous dispersion region of tellurite HF for different launched average pump powers (top: fiber length 1.35m; bottom: fiber length 0.5m). The vertical lines represent the individual positions of the first order Stokes/anti-Stokes and second order Raman Stokes peaks corresponding to the 741cm^{-1} Raman line. The dashed line at 1.38μm represents the ZDW of tellurite ASC HF.

D. Extending SC into the anomalous dispersion region

Fig.8 shows the SC extending across 1.38μm and into the anomalous dispersion region with higher launched average pump power. It is seen that by increasing the launched average pump power to 128.7mW, corresponding to a peak power of 447W, the 10dB-bandwidth of the generated continuum from 1.35m-long and 0.5m-long HF is ~600nm and ~200nm, respectively. Note that the spectrum beyond 1700nm could not be observed due to the limited range of the OSA. Such broadband SC observed in the longer HF is because of the generated third-order Raman Stokes at a wavelength around ZDW, subsequently acts as a pump for SC generation within the near zero dispersion/anomalous dispersion pump scheme. In this regime, a combination of nonlinear effects including four wave mixing, modulation instability and soliton-related dynamics broaden the spectrum significantly [18, 19].

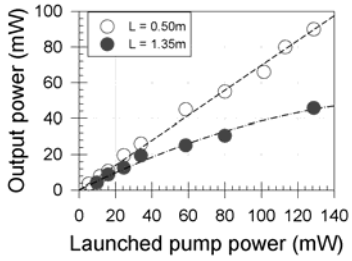

Fig.9: Measured average output powers vs launched average pump powers (L: the used fiber length)

The relation between the average output powers and launched average pump powers in the fibers with 1.35m and 0.50m length is shown in Fig.9. For the 0.50m-long HF, the output and the pump power show a good linear relation with a nearly constant 68% conversion efficiency. For the 1.35m-long HF, the pump-to-SC conversion efficiency appears nonlinear: at low pump power levels, i.e., when the launched average pump power is less than 33.9mW and the generated Raman stokes is within the normal dispersion region, the slope of the conversion efficiency is ~50%; at high pump power, where the generated SC extends across the ZDW of the fiber, the conversion efficiency decreases significantly, dropping to 36% at an average pump power of 128.7mW. The decrease of the conversion efficiency of the 1.35m-long fiber in comparison with the 0.50m long fiber is likely because (1) there exists an additional propagation loss of 1.8dB for the 1060nm pump in the longer fiber, and (2) the quantum defect from the pump photons to the generated photons significantly increases when the SC crosses the ZDW and extends towards much longer wavelengths. By contrast, for the 0.50m long fiber the spectrum is essentially composed of SRS peaks between 1.15-1.20μm so that the quantum defect is low.

E. Numerical simulation of SRS and SCG in tellurite HF

In order to confirm our understanding of the above experimental results, we performed numerical simulations of SRS and SC generation in the tellurite ASC HF. The simulations solve the generalized nonlinear Schrödinger equation using a split-step Fourier technique. A sufficiently large number of discretization points were chosen to ensure appropriate coverage of the large temporal and spectral windows. The model used as inputs the measured Raman gain (Table 1), Raman spectrum (Fig.1), mode area (Fig.2), fiber dispersion (Fig.4), and input pump spectrum (Fig.6). In the time domain the pump pulses were modeled with a Gaussian shape of 20ps pulse duration. Due to the flat loss spectrum of the HF from 1.0-1.65μm, in the simulation, a constant loss value of 2.3dB/m was set in the simulation.

Fig.10 illustrates the calculated SRS and SC generated from the 1.35m-long (top) and 0.5m-long (bottom) fiber, for average pump powers of ~3mW, 9mW, 15mW, 21mW, and 30mW, corresponding to peak powers of 10W, 30W, 50W, 70W, and 100W, respectively. The simulated spectra show more pronounced peaks than the measured curves, but overall the spectral profiles correspond well with the experimental results.

However, we note that the powers used in the experiment were about 3-4 times higher than the powers used in the simulations for generating similar spectra. For example, the experimental SC generated in the 1.35m-long HF under the launched average pump power of 128.7mW (see Fig.8 (top)) is similar to the simulated SC under the launched average pump power of 30mW (see Fig.10 (top)), in terms of their spectral line-shape and the bandwidth. We attribute this discrepancy mainly to the idealized Gaussian pulse shape used in the simulations, which neglects pulse distortions prior to the fiber launch and for example any long temporal pedestals. The significantly enhanced undepleted pump power in the output

spectra observed in the experiments compared to the simulations supports this argument.

In addition, an extra simulation was run to investigate the impact of SPM effect in comparison with the Raman effect on the SC generated in the fiber under the experimental conditions. Generally it is not possible to separate for example SPM from FWM in the simulation. Instead, the Raman effect in the simulation was intentionally switched off in the model. This leaves all the Kerr nonlinearities (including SPM, FWM and so on) intact. So under an average pump powers of 30mW (corresponding to a peak powers of 100W), for the 1.35m-long fiber, the outcome trace is very similar to the original pump and the broadening of the spectrum is minor due to the highly normal dispersion at the pump wavelength. It indicates that at the initial broadening stage of the spectrum when the generated SC is within the highly normal dispersion regime, no significant broadening occurs without the assistance of the Raman effect. Therefore the SPM effect does not play a significant role in such a situation. Of course, once the SC is close to and/or crosses the ZDW, all the nonlinear effects contribute significantly to the SC.

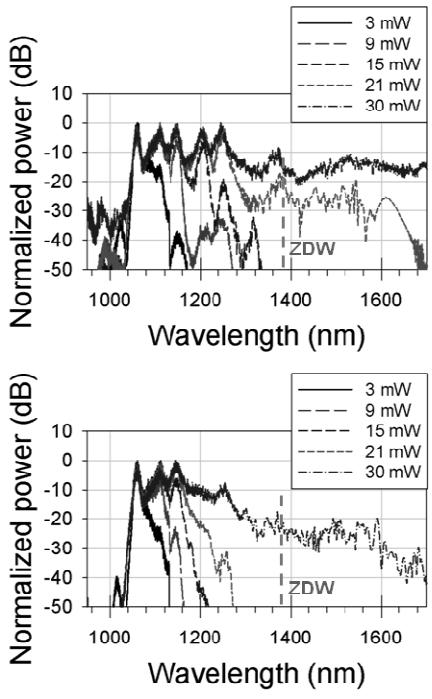

Fig.10: Simulated SRS and SC generated in tellurite HF with lengths of 1.35m (top) and 0.50m (bottom), for launched average pump powers of 3mW, 9mW, 15mW, 21mW, and 30mW, respectively. The dashed line at 1.38μm represents the ZDW of tellurite ASC HF.

Fig.11 shows the calculated conversion efficiency from the average pump power to the average SC output power. When the average launched power increases from 3mW to 30mW, the conversion efficiency in the 0.5m-long fiber decreases from 77% to 71%, while for the 1.35m-long fiber the conversion efficiency decreases from 49% to 42%. These numbers compare well with the experimental results, considering the differences in launched pump power as discussed above.

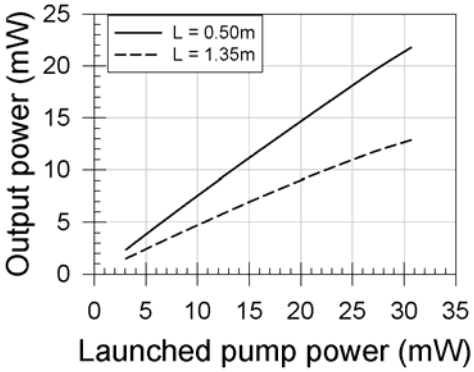

Fig.11: Calculated average output powers vs launched average pump powers

V. Perspective of Power Scaling for High Power SC Applications

Even higher SC output power could not be achieved in the experiment due to the damage of the input facet of the HF when the launched average pump power reached ~140mW (corresponding to a peak power of 390W). Fig.12 shows optical photographs of the cross section of the ASC HF before and after the facet damage. It can be seen that in the damaged fiber the air-suspended-core has disappeared but the three supporting spokes still exist. Such damage was observed reproducibly under the same launched average pump power level. The damage intensity is estimated to be 18.7GW/cm^2. The surface damage threshold of tellurite bulk glasses was reported to be 15-20GW/cm^2 using a Nd:YAG laser at 1064nm with a similar pulse duration of 25ps [5]. Note that this reported surface damage threshold of bulk glass was measured before the light was launched into the glass; thus the combined Fresnel reflection loss, which is ~20% if the light is at near-normal incidence to the interface, was not taken into account. Therefore, the damage threshold obtained from our experiment is comparable to the reported value of the bulk.

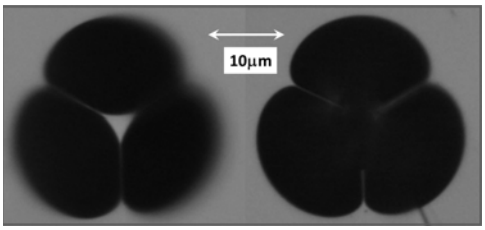

Fig.12: Optical microscopic images at the input end of the tellurite ASC HF before (left) and after (right) the damage

Power scaling is always desired for a practical laser source. For rare-earth doped fiber lasers or Raman fiber lasers, power scaling of the laser requires scaling up the core diameter of the fiber. However, for a fiber-based supercontinuum source with pumping near the ZDW, the dispersion profile plays a dominant role for the spectrum profile and the SC bandwidth. Unfortunately, using the same core material the dispersion profile of a large-core fiber will be totally different from that of a small-core fiber. The former dispersion will be very close to the material dispersion, while the latter one will exhibit a ZDW shifted to a much shorter wavelength due to the large waveguide dispersion. From Fig.4 one can see such a

difference in dispersion between a small-core tellurite fiber and a large-core tellurite fiber. As a result, power scaling is difficult to achieve using the anomalous dispersion pumping scheme. For the normal dispersion pumping scheme, on the other hand, dispersion becomes less problematic. If we use a large-core tellurite fiber, more cascaded Raman Stokes orders are required before they reach and cross the ZDW (~2μm) of the fiber, but the general mechanisms for generating a broadband SC are the same as in the small-core fiber. In this case, much higher output power can be obtained without fiber damage. For example, if we consider a large-core tellurite fiber with a large effective mode area A_{eff} of 500μm^2 at 1060nm, we deduce that the launched average power causing facet damage will be as high as 27W. Note that a very large mode area tellurite HF with A_{eff} of 3000μm^2 has already been demonstrated [20].

We performed numerical simulations to confirm the power scalability of SC in tellurite fiber. Fig.13 shows simulation results for a 1m-long (top) and 2m-long (bottom) tellurite LMA fiber with A_{eff} = 500μm^2. The fiber loss is assumed to be 1 dB/m at 1060nm and the dispersion is assumed to follow the bulk material dispersion with a ZDW of 2.15μm. The same pump source properties were chosen as for the simulations in Fig.10 but were scaled to higher powers. The launched average power was set as 0.6W, 3.0W, 6.0W, 9.6W, 12W and 15W, corresponding to peak powers of 2kW, 10kW, 20kW, 32kW, 40kW and 48kW, respectively. Fig. 13 shows that broadband SC spanning from 1.1μm to 1.7μm with 10dB bandwidth can be respectively generated from 1m-long and 2m-long LMA tellurite fibers.

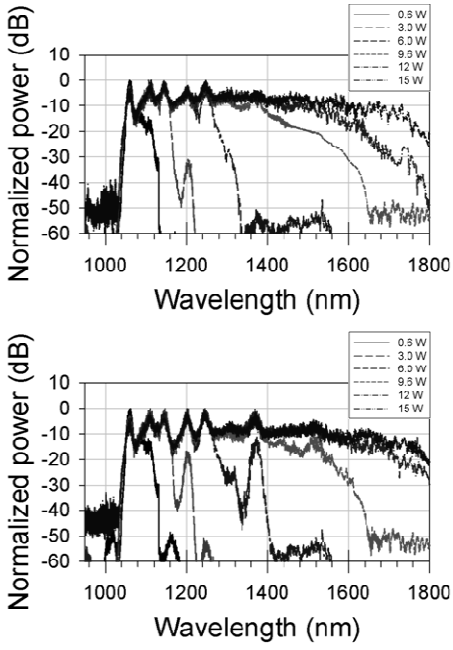

Fig.13: Simulated SC generated in LMA (A_{eff} = 500μm^2) tellurite HF with lengths of 1m (top) and 2m (bottom) for launched average pump powers of 0.6W, 3.0W, 6.0W, 9.6W, 12W, and 15W.

Fig.14 shows the calculated average output power and conversion efficiency as a function of launched average pump powers for 1m-, and 2m- long LMA tellurite fibers. It can be noted that there is no significant improvement by using 2m-long fiber in comparison with using 1m-long fiber, due to the walk-off effect. More than 60% conversion efficiency can be expected in a 1m-long fiber when the average launched power increases up to 15W. In other words, a SC from 1.1-1.7μm, i.e., with a 10dB-bandwidth of ~600nm and with an average output power of 9.5W, corresponding to a mean spectral density of 15mW/nm, can be achieved in a 1m-long LMA tellurite fiber. Hence, a LMA tellurite HF is a promising candidate for generating watt-level near-IR SC using the normal dispersion pumping scheme. Though the SC bandwidth using the normal dispersion pumping scheme here is not as great as the one obtained from 1550nm anomalous dispersion pumping [21], the high average power of SC output, the high spectral intensity, and the high pump-to-SC conversion efficiency in this work indicate the promise of generating high average power near-infrared (1-1.7μm) SC source.

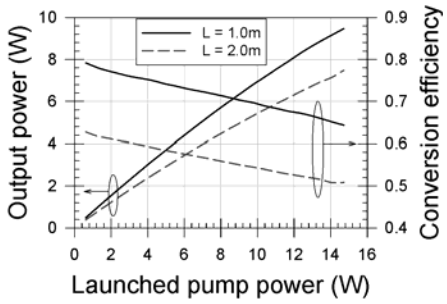

Fig.14 Calculated output average powers vs launched average pump powers and conversion efficiency vs launched average pump powers with the 1m-, and 2m- long , LMA (A_{eff} = 500μm^2) tellurite HF respectively.

VI. Conclusion and Future Work

In summary, we have experimentally investigated Raman-assisted broadband near-infrared supercontinuum generation in a single-mode tellurite ASC HF with lengths of 1.35m and 0.50m, pumped by a 20ps pulsed laser in the highly normal dispersion region. The spectral broadening is mainly attributed to the high Raman gain coefficient and the broadband Raman bands of the tellurite glass. With this normal dispersion pumping scheme, we expect that power scaling should be possible to generate broadband infrared 1.1-1.7μm SC with output average powers as high as 10W and mean spectral density of 15mW/nm in a 1m-long large mode area tellurite fiber with a mode area of 500μm^2. It proves that the normal dispersion pumping scheme using 1.06μm pulsed laser is a viable approach to achieve broadband and potentially high-power output supercontinuum in tellurite fiber.

VII. Acknowledgment

The authors would like to thank Dr. Dejiao Lin for the help with operating the source. Jindan Shi gratefully acknowledges the China Scholarship Council for financial support. Morten Ibsen acknowledges the Royal Society of London for the provisioning of a University Research Fellowship.

REFERENCES

[1] R. R. Alfano, Editor, "The Supercontinuum Laser Source," 2nd Ed., Springer, 2005.

[2] J. K. Ranka, R. S. Windeler, and A. J. Stentz, "Visible continuum generation in air silica microstructure optical fibers with anomalous dispersion at 800 nm," Opt. Lett., **25**(1), pp. 25-27, 2000.

[3] J. C. Knight, T. A. Birks, P. St. J. Russell and D. M. Atkin, "All-silica single-mode fiber with photonic crystal cladding," Opt. Lett., **21**(19), pp. 1547-1549, 1996.

[4] G. P. Agrawal, Nonlinear Fiber Optics, 3rd Ed. Academic, San Diego, (2000).

[5] R. Stegeman, L. Jankovic, H. Kim, C. Rivero, G. Stegeman, K. Richardson, P. Delfyett, Y. Guo, A. Schulte, and T. Cardinal, "Tellurite glasses with peak absolute Raman gain coefficients up to 30 times that of fused silica," Opt. Lett., **28**(13), pp. 1126-1128, 2003.

[6] L. L. Chase and E. W. V. Stryland, "Nonlinear optical properties" in Handbook of laser science and technology supplement 2: Optical materials, M. J. Weber, ed. (CRC Press), Section 8.

[7] G. Ghosh, "Sellmeier coefficients and chromatic dispersions for some tellurite glasses," J. Am. Ceram. Soc., **78**(10), pp. 2828-2830, 1995.

[8] M. Liao, C. Chaudhari, G. Qin, X. Yan, T. Suzuki and Y. Ohishi, "Tellurite microstructure fibers with small hexagonal core for supercontinuum generation," Opt. Express, **17**(14), pp. 12174-12182, 2009.

[9] J. S. Wang, E. M. Vogel, and E. Snitzer, "Tellurite glass: a new candidate for fiber devices," Opt. Mater, **3**(3), pp. 187-203, 1994.

[10] X. Feng, T. M. Monro, V. Finazzi, R. C. Moore, K. Frampton, P. Petropoulos, D. J. Richardson, "Extruded singlemode, high-nonlinearity, tellurite glass holey fibre," Electron. Lett., **41**(15), pp. 835-837, 2005.

[11] R. Shuker and R. W. Gammon, "Raman scattering selection rule breaking and density of states in amorphous materials," Phys. Rev. Lett., **25**(4), pp. 222–225, 1970.

[12] V. G. Plotnichenko, V. O. Sokolov, V. V. Koltashev, E. M. Dianov, I. A. Grishin and M. F. Churbanov, "Raman band intensities of tellurite glasses," Opt. Lett., **30**(10) , pp. 1156-1158, 2005.

[13] R.H.Stolen and E.P. Ippen, "Raman gain in glass optical waveguides," Appl. Phys. Lett., **22**(6), pp. 276-278, 1973.

[14] F. L. Galeener,J. C. Mikkelsen, R. H. Geils and W. J. Mosby, "The relative Raman cross sections of vitreous SiO_2, GeO_2, B_2O_3, and P_2O_5," Appl. Phys. Lett., **32**(1), pp. 34-36, 1978.

[15] C. Rivero, K. Richardson, R. Stegeman, G. Stegeman, T. Cardinal, E. Fargin, M. Couzi, V. Rodriguez, "Quantifying Raman gain coefficients in tellurite glasses," J. Non-Cryst. Solids, **345&346**, pp. 396–401, 2004.

[16] K. Chen, J. H. V. Price, S. Alam, J. R. Hayes, D. Lin, A. Malinowski, and D. J. Richardson, "Polarisation maintaining 100W Yb-fiber MOPA producing μJ pulses tunable in duration from 1 to 21 ps,", Opt. Express, **18**(14), pp.14385-14394, 2010.

[17] K. Chen, S. Alam, P. Horak, C. A. Codemard, A. Malinowski, and D. J. Richardson, "Excitation of individual Raman Stokes lines in the visible regime using rectangular-shaped nanosecond optical pulses at 530 nm," Opt. Express, **35**(14), pp. 2433-2435, 2005.

[18] J. M. Dudley, G. Genty, and S. Coen, "Supercontinuum generation in photonic crystal fiber," Rev. Mod. Phys., **78**(4), pp. 1135-1184, 2006.

[19] A. K. Abeeluck and C. Headley, "Continuous-wave pumping in the anomalous- and normal-dispersion regimes of nonlinear fibers for supercontinuum generation," Opt. Lett., **30**(1), pp. 61-63, 2005.

[20] X. Feng, W. H. Loh, J. C. Flanagan, A. Camerlingo, S. Dasgupta, P. Petropoulos, P. Horak, K. E. Frampton, N. M. White, J. H.V.Price, H. N. Rutt, and D. J. Richardson, "Single-mode tellurite glass holey fiber with extremely large mode area for infrared nonlinear applications," Opt. Express, **16**(18), 3651-3656, 2008.

[21] T. Delmonte, M. A. Watson, E. J. O'Driscoll, X. Feng, T. M. Monro, V. Finazzi, P. Petropoulos, J. H. V. Price, J. C. Baggett, W. H. Loh, D. J. Richardson, D. P. Hand, "Generation of mid-IR continuum using tellurite microstructured fiber," in the proceedings of CLEO/QELS, 2006, Paper CTuA4.

Jindan Shi was born in Zhejiang, China. She received a B.Sc. degree with honors in telecommunication engineering from Beijing University of Post and Telecommunications (BUPT), China, in 2006. From October 2008, she is a Ph.D. student at the Optoelectronics Research Centre (ORC), Southampton, UK. Her research currently focuses on periodic fiber devices for advanced applications in all optical systems.

Xian Feng

Peter Horak

Kangkang Chen

Peh Siong Teh

Shaif-ul Alam

Wei H. Loh

David J. Richardson

Morten Ibsen